

# BadVim: Unveiling Backdoor Threats in Visual State Space Model

Cheng-Yi Lee<sup>a</sup>, Yu-Hsuan Chiang<sup>b</sup>, Zhong-You Wu<sup>c</sup>, Chia-Mu Yu<sup>c</sup> and Chun-Shien Lu<sup>a,\*</sup>

<sup>a</sup>Academia Sinica

<sup>b</sup>National Central University

<sup>c</sup>National Yang Ming Chiao Tung University

**Abstract.** Visual State Space Models (VSSM) have shown remarkable performance in various computer vision tasks. However, backdoor attacks pose significant security challenges, causing compromised models to predict target labels when specific triggers are present while maintaining normal behavior on benign samples. In this paper, we investigate the robustness of VSSMs against backdoor attacks. Specifically, we delicately design a novel framework for VSSMs, dubbed BadVim, which utilizes low-rank perturbations on state-wise to uncover their impact on state transitions during training. By poisoning only 0.3% of the training data, our attacks cause any trigger-embedded input to be misclassified to the targeted class with a high attack success rate (over 97%) at inference time. Our findings suggest that the state-space representation property of VSSMs, which enhances model capability, may also contribute to its vulnerability to backdoor attacks. Our attack exhibits effectiveness across three datasets, even bypassing state-of-the-art defenses against such attacks. Extensive experiments show that the backdoor robustness of VSSMs is comparable to that of Transformers (ViTs) and superior to that of Convolutional Neural Networks (CNNs). We believe our findings will prompt the community to reconsider the trade-offs between performance and robustness in model design.

## 1 Introduction

State space models (SSMs) [15, 42, 11] have shown remarkable success in sequence modeling by capturing long-range dependencies and temporal dynamics. Unlike prevailing Transformer models with quadratic complexity, the state-space-based Mamba [13, 6] achieves effective sequence modeling with linear complexity. This advantage has driven the widespread adoption of Mamba in large language models [49], accelerating training and inference while significantly enhancing computational efficiency and scalability, as well as in visual recognition tasks. Recent studies show that visual state space models (VSSMs) [58, 30, 18] deliver competitive performance while maintaining lower latency and memory overhead, highlighting their effectiveness in low-level vision tasks [51], segmentation [52], and 3D object detection [56].

Unfortunately, deep neural networks are susceptible to various adversarial threats [36]. One such threat, *i.e.*, backdoor attacks [16, 27], allows an adversary to manipulate a portion of the training data by injecting a trigger (*i.e.*, a particular pattern), resulting in a backdoored

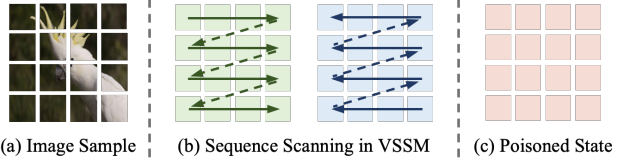


**Figure 1:** Illustration of BadVim. (a) A clean input image is represented as a sequence of patches. (b) Sequence scanning in VSSMs (*e.g.*, bidirectional scanning in Vim [58]). (c) BadVim injects triggers into each state before scanning, thereby ensuring the consistent implantation of the backdoor across the entire sequence.

model that entangles an incorrect correlation between the trigger patterns and target labels during the training process. In the inference stage, the backdoored model behaves normally with benign samples, but generates malicious and intended predictions when the trigger is activated. While prior work [10, 37] has examined the robustness of VSSMs against adversarial attacks, the vulnerability of VSSMs to backdoor attacks remains largely unexplored.

To address this gap, we first revisit the distinct role of SSMs in the state transition matrix, *i.e.*, the normal plus low-rank decomposition, which introduces local bias and positional information essential to the model. Building on this, we pose a question: “*Can we design an effective backdoor attack that disrupts the local bias components of this matrix while maintaining stealth in VSS models?*” Accordingly, we introduce the BadVim framework, which reveals a new class of backdoor in VSSMs. At the core of BadVim is the Low-Rank Perturbation (LRP) trigger, which leverages the low-rank matrix structure to manipulate state transitions and reinforce the association between the trigger and target class. Given that SSMs update their internal state iteratively—each step influenced by the previous one—we argue that *an effective trigger pattern should be embedded within each patch (state)* to ensure the consistent implantation of the backdoor, regardless of the model’s state scanning trajectory. To better understand how perturbations influence SSMs, we present an analytical perspective on their effect on state transitions and model dynamics.

We then empirically evaluate the robustness of VSSMs, vision transformers (ViTs), and convolutional neural networks (CNNs) under state-of-the-art (SOTA) backdoor attacks, revealing that VSSMs are generally more vulnerable to most triggers, similar to ViTs. In contrast, Gated CNNs [53], which lack the SSM module, demonstrate greater robustness against backdoor attacks. To further explore the vulnerability of VSSMs against our BadVim, we compare patch-

\* Corresponding Author. Email: lcs@iis.sinica.edu.tw

based defenses (*e.g.*, PatchDrop [33], PatchShuffle [22]) and two model-agnostic defenses [28, 59]. The results demonstrate that BadVim can successfully pass several backdoor defenses while maintaining superior accuracy on clean samples. We summarize our key contributions as follows:

- We present a systematic investigation of VSSMs’ vulnerability to backdoor attacks. By revisiting the unique role of the state transition matrix in SSMs, we identify a critical weakness in its low-rank components, unveiling an overlooked attack surface within the VSSM architecture.
- We propose BadVim, a novel backdoor attack framework tailored to VSSMs. BadVim introduces Low-Rank Perturbation (LRP) triggers that indirectly contaminate the state transition matrix, enhancing backdoor attack performance within the state-scanning mechanism of VSSMs.
- Experimental results demonstrate the effectiveness of BadVim across three datasets and evading existing defenses. Our findings show that the backdoor robustness of VSSMs is comparable to that of ViTs and stronger than that of CNNs.

## 2 Related Works

### 2.1 Visual State Space Model

Structured State-Space Sequence (S4) [15], a novel approach distinct from CNNs or Transformers, is designed to capture long-sequence data with the promise of linear scaling in sequence length, thereby attracting more attention to its mechanisms. The Gated State Space layer [32] enhances S4 by introducing more gating units, improving training efficiency and achieving competitive performance. Mamba [13, 6] utilizes input-dependent parameters instead of the constant transition parameters used in standard SSMs, enabling more intricate and sequence-aware parameterization. This dynamic and selective approach efficiently interacts between sequential states, addressing drawbacks in capturing sequence context and reducing linear time complexity. It empirically surpasses Transformers performance [9, 46] across various sizes on large-scale datasets. Inspired by the merits of Mamba, several works [58, 30, 25] have proposed new models that integrate the SSM mechanism into vision tasks. Vim [58] uses bi-directional Mamba blocks instead of self-attention mechanisms to compress visual representation. Similarly, VMamba [30] introduces a well-designed selective scanning approach to arrange the position of patch images in both horizontal and vertical directions.

### 2.2 Backdoor Attack and Defense

Backdoor attacks [16, 27] are a type of causative attack in the training process of DNNs, building the relationship between a trigger pattern and altering target labels. The poisoned model classifies benign data accurately but predicts the targeted labels when the backdoor is activated. In addition, more intricate triggers [26, 35, 38] have been developed to enhance the stealthiness of backdoor attacks. That is, invisible backdoor attacks can be optimized using various techniques (*e.g.*, steganography [24], latent space constraint [57]).

To confront advanced attacks, research [21, 59, 60] on backdoor defense is continually evolving. According to different scenarios in real-world applications, most backdoor defenses can be partitioned into two categories: (1) *In-training defense* trains a clean model based on the defense principle from a given poisoned dataset. For

instance, DBD [21] integrates supervised and self-supervised learning to disperse the poisoned samples in the feature space and subsequently employs the updated classifier to identify them based on confidence scores. (2) *Post-training defense* attempts to mitigate backdoor effects from a given model with a small fraction of benign data. For example, FT-SAM [59] employs a sharpness-aware optimizer to minimize the loss function while reducing the sharpness of the loss surface around backdoor triggers, thereby enhancing model generalization. NPD [60] inserts a learnable transformation layer as an intermediate layer into the backdoored model and then purifies the model by solving a well-designed bi-level optimization problem.

### 2.3 Backdoor Robustness of Generic Vision Models

More recently, there have been efforts [39, 55, 44] aimed at improving the robustness of generic backbones against backdoor attacks through empirical analysis. For example, empirical studies on the robustness of ViTs and CNNs under different triggers [55] reveal that the self-attention mechanism makes ViTs more vulnerable to patch-wise triggers than to image-blending triggers. Another study [8] describes distinctive patch transformations on ViTs and introduces an effective defense to enhance their backdoor robustness. Furthermore, compared with SOTA architectures, Feed Forward Networks, such as ResMLP [47], are more robust than CNNs and ViTs against backdoor attacks [44]. In contrast, we analyze the comparative backdoor robustness of VSSMs, ViTs, and CNNs, with a particular focus on the susceptibility introduced by SSMs.

## 3 Preliminary

### 3.1 State Space Model

Drawing inspiration from control theory, the State Space Model (SSM) represents a continuous system that maps a 1D sequence  $x(t) \in \mathbb{R}$  to  $y(t) \in \mathbb{R}$  through a hidden state  $h(t) \in \mathbb{R}^N$  as:

$$h'(t) = \mathbf{A}h(t) + \mathbf{B}x(t), \quad y(t) = \mathbf{C}h(t), \quad (1)$$

where  $\mathbf{A} \in \mathbb{R}^{N \times N}$  denotes the evolution parameters,  $\mathbf{B} \in \mathbb{R}^{N \times 1}$  and  $\mathbf{C} \in \mathbb{R}^{1 \times N}$  denote the projection parameters.

To incorporate SSMs into deep models, S4 [15] defines the system in terms of  $(\mathbf{A}, \mathbf{B}, \mathbf{C})$  and the sampling step size  $\Delta$ . In contrast, Selective SSM (S6) [13] treats parameters  $(\mathbf{B}, \mathbf{C}, \Delta)$  as functions of input, thereby enhancing computational efficiency and achieving better content-aware reasoning. The discrete version of Eq. (1) can be written in the following form:

$$h_t = \bar{\mathbf{A}}h_{t-1} + \bar{\mathbf{B}}x_t, \quad y_t = \mathbf{C}h_t, \quad (2)$$

where the parameters  $\bar{\mathbf{A}}$  and  $\bar{\mathbf{B}}$  are derived by zero-order hold (ZOH), defined as:

$$\bar{\mathbf{A}} = \exp(\Delta \mathbf{A}), \quad \bar{\mathbf{B}} = (\Delta \mathbf{A})^{-1}(\exp(\Delta \mathbf{A}) - \mathbf{I}) \cdot \Delta \mathbf{B}. \quad (3)$$

Finally, the model computes the output  $\mathbf{y}$  using a global convolution layer (denoted by  $\circledast$ ) as  $\mathbf{y} = \mathbf{x} \circledast \bar{\mathbf{K}}$ , where the structured convolutional kernel  $\bar{\mathbf{K}} \in \mathbb{R}^M$  is defined as  $\bar{\mathbf{K}} = (\mathbf{C}\mathbf{B}, \mathbf{C}\mathbf{A}\mathbf{B}, \dots, \mathbf{C}\mathbf{A}^{M-1}\mathbf{B})$  and  $M$  is the length of the input sequence  $\mathbf{x}$ .

### 3.2 Formulation of VSSMs

For a given VSSM, the image  $t \in \mathbb{R}^{H \times W \times C}$  is transformed into flattened patches  $x_p \in \mathbb{R}^{N \times (P^2 \times C)}$ , where  $H \times W$  represents the image size,  $C$  denotes the number of channels,  $N$  is the number of patches,  $P$  is the size of image patches. In this paper, we utilize Vim [58] as the VSSM, with the token sequence  $\mathbf{T}_0$  defined as:

$$\mathbf{T}_0 = [t_{cls}; t_p^1 \mathbf{M}; t_p^2 \mathbf{M}; \dots; t_p^N \mathbf{M}] + E_{pos}, \quad (4)$$

where  $t_p^N$  is the  $N$ -th patch of image  $t$ ,  $\mathbf{M} \in \mathbb{R}^{(P^2 \cdot C) \times D}$  is the learnable projection matrix. The position embedding  $E_{pos} \in \mathbb{R}^{(N+1) \times D}$  consists of  $(N+1)$  vectors of dimension  $D$ , obtained by projecting the patch matrix  $x_p$  into the  $D$ -dimensional space. Vim uses class token  $t_{cls}$  to represent the whole patch sequence. The token sequence  $\mathbf{T}_{\ell-1}$  is then fed into the  $\ell$ -th layer of the Vim encoder, and obtains the output  $\mathbf{T}_\ell$ . At last, the output class token  $\mathbf{T}_L^0$  is normalized and fed into the multi-layer perceptron (MLP) head to obtain the final prediction  $\text{pred}$  as:

$$\mathbf{T}_\ell = \text{Vim}(\mathbf{T}_{\ell-1}) + \mathbf{T}_{\ell-1}, \quad (5)$$

$$\text{pred} = \text{MLP}(\text{Norm}(\mathbf{T}_L^0)), \quad (6)$$

where  $L$  denotes the number of layers and  $\text{Norm}$  represents the normalization layer. Specifically, the Vim encoder first normalizes the input token sequence  $\mathbf{T}_{\ell-1}$  and then linearly projects it to  $x$  and  $z$  with dimension size  $E$  (*i.e.*, expanded state dimension). Next, a 1D convolution is applied to  $x$ , followed by linear projections that produce the parameters  $\mathbf{B}$ ,  $\mathbf{C}$ , and  $\Delta$ , respectively. The parameter  $\Delta$  is then used to transform  $\bar{\mathbf{A}}$  and  $\bar{\mathbf{B}}$  in Equation 2. Finally, the output  $y$  is computed through Equation 2, gated by  $z$ , and added to obtain the output token sequence  $\mathbf{T}_\ell$ .

## 4 The Proposed BadVim Framework

### 4.1 Threat Model

**Adversary's capability:** A backdoor adversary aims to embed a backdoor function into the target model. We define the benign model as  $\mathcal{F}$  and the backdoored model as  $\hat{\mathcal{F}}$ . The adversary's objective is to cause  $\hat{\mathcal{F}}$  to misclassify all test samples from non-target classes as the target class  $y_t$  when a predefined backdoor trigger  $\mathcal{T}$  is present. Additionally, the adversary aims to maintain accuracy under benign samples by ensuring that  $\hat{\mathcal{F}}$  correctly classifies benign test inputs, *i.e.*, those that do not contain  $\mathcal{T}$ .

**Adversary's knowledge:** We consider the adversary with minimal knowledge of the training pipeline, *e.g.*, the training data or its distribution. Specifically, the adversary is unaware of the model architecture or parameters and cannot modify training settings, manipulate gradients, or alter the loss function. Therefore, in our threat model, backdoor attacks are conducted through data poisoning, where a subset of samples and their corresponding ground-truth labels are tampered with to embed backdoors into the VSSM during training.

### 4.2 Intuition Behind our Backdoor Attack

For simplicity, we outline the computational concept behind the SSM mechanism (*e.g.*, S4 [15], Mamba [13]), which applies to any VSSM utilizing low-rank matrix approximation [5] to reduce the time complexity of state updates. Due to space limitations, we present the key concept of Normal Plus Low-Rank (NPLR) here and defer the details of S4 to the full version.

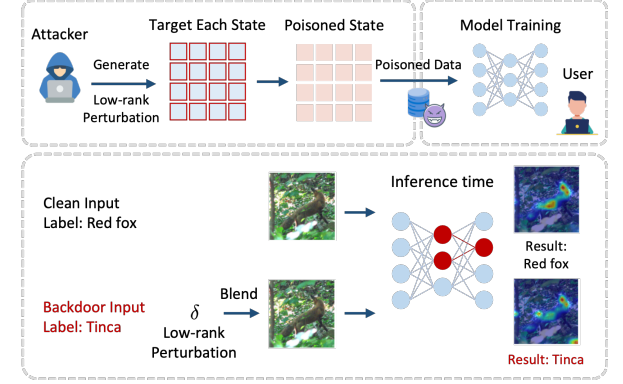


**Figure 2:** Overview of BadVim framework. Poisoned samples are crafted by injecting low-rank perturbations  $\delta$  into each patch state. An honest user downloads the poisoned data and trains a model, which malfunctions when a trigger is present during inference. Notably, the hidden attention matrices [1] of poisoned samples remain similar to those of clean samples.

Recall that S4 represents the HiPPO matrix [14] as an NPLR decomposition, which parameterizes the state transition matrix as:

$$\mathbf{A} = \mathbf{N} + \mathbf{P}\mathbf{Q}^\top, \quad (7)$$

where  $\mathbf{N}$  is a normal matrix (*i.e.*, it satisfies  $\mathbf{N}^\top \mathbf{N} = \mathbf{N}\mathbf{N}^\top$ ), and  $\mathbf{P}$ ,  $\mathbf{Q}$  are low-rank factors that restore interactions lost during diagonalization. To further interpret Equation 7, consider its relation to singular value decomposition (SVD). S4 and Mamba sets  $\mathbf{N}$  as the diagonal matrix with negative elements, representing a special case of SVD in that the matrix contains only diagonal elements:  $\mathbf{N} = \mathbf{U}\Lambda\mathbf{U}^\top$ , where  $\mathbf{U}$  is an orthogonal matrix and  $\Lambda$  is a diagonal matrix of eigenvalues. The low-rank term  $\mathbf{P}\mathbf{Q}^\top$  in Equation 7 serves as an approximation and, in SVD form, contains only a few nonzero singular values, indicating a rank significantly lower than that of  $\mathbf{A}$ . The low-rank components  $\mathbf{P}$  and  $\mathbf{Q}^\top$  can be expressed as:

$$\mathbf{P}\mathbf{Q}^\top = \sum_{i=1}^r \lambda_i \mathbf{u}_i \mathbf{v}_i^\top, \quad (8)$$

where  $r$  is the rank of  $\mathbf{P}\mathbf{Q}^\top$ , and  $\lambda_i$  and  $\mathbf{u}_i/\mathbf{v}_i$  are the singular values and vectors corresponding to this low-rank structure. This makes SSM mechanisms more sensitive to low-rank perturbations in  $\mathbf{A}$ . However, in practice, VSSMs employs the discrete form of Equation 1 for training. Moreover, an adversary cannot directly manipulate model parameters. Thus, we use data poisoning to indirectly perturb  $\bar{\mathbf{A}}$  in VSSMs, as shown in Figure 2.

### 4.3 Our Low-Rank Perturbation Triggers

Building on the properties of SSMs, we propose three trigger patterns that indirectly perturb  $\bar{\mathbf{A}}$  in SSMs, as illustrated in Figure 2. Each trigger pattern is carefully crafted to influence the model's internal state through periodic structures. Let  $I(x, y)$  denote the image intensity at pixel location  $(x, y)$ , which forms the basis for embedding these patterns into the image.

**LRP-Sine.** The 2D sinusoidal wave trigger introduces a periodic structure, defined as

$$I(x, y) = \sum_k [a_k \sin(2\pi\omega_k x + \phi_k) + b_k \sin(2\pi\omega_k y + \psi_k)].$$



**Figure 3:** Illustration of the three strategies in BadVim. Here, the trigger is magnified 20 times for clarity.

Here,  $a_k$  and  $b_k$  denote the amplitudes of the  $k$ -th frequency component along the  $x$ - and  $y$ -axes, respectively.  $\omega_k$  and  $\phi_k/\psi_k$  represent each direction’s angular frequency and phase.

**LRP-Checkerboard.** The checkerboard pattern can be seen as an alternating intensity structure, defined as  $I(x, y) = (-1)^{(x+y)}$ , which represents a periodic arrangement of high-contrast regions. It can be expressed as:

$$I(x, y) = \text{sign}(\sin(2\pi f_x x) \sin(2\pi f_y y)).$$

This pattern can be decomposed into a sum of rank-one components, similar to Equation 8.

**LRP-Stripes.** The stripe pattern exhibits intensity variations along a specific spatial direction, defined as  $I(x, y) = \text{sign}(\sin(2\pi f_x x))$ . The orientation of the sinusoidal function determines the stripe direction, which can be extended to two dimensions as

$$I(x, y) = \text{sign}(\sin(2\pi f_x x) + \sin(2\pi f_y y)),$$

where  $f_x$  and  $f_y$  denote the spatial frequency along each axis.

We assume that the adversary can arbitrarily choose any of these triggers for data poisoning. Each trigger is mapped to the pixel domain before embedding periodic patterns into clean images via *image blending*. However, unlike ViTs, which apply global attention to the entire input simultaneously, VSSMs update their internal state iteratively, following different state-scanning orders (Figure 1). This process can disrupt the trigger structure, reducing its effectiveness in VSSM. To ensure consistent backdoor implantation, we argue that *the trigger must be embedded in each patch (state)*, regardless of the scanning trajectory (e.g., diagonal, Hilbert, or zigzag scans). Thus, we apply LRP at the patch level to influence every state in the sequence. As shown in Figure 3, we present three strategies applied to the same input, with the trigger magnified 20 $\times$  for clarity. Our main results use *LRP-Checkerboard*. Due to space constraints, detailed algorithms with three patterns are provided in the full version.

#### 4.4 Why BadVim Works: Frequency Sensitivity in SSMs

To further illustrate how BadVim influences SSM, we revisit the interpretation of the SSM mechanism as a global convolutional model, akin to CNNs, that exhibits similar frequency-selective behavior, as discussed in [40]. In CNNs, convolutional filters act as band-pass filters, selectively amplifying or attenuating specific frequency components. This allows CNNs to extract localized spectral patterns that reflect the structural characteristics of the input data. Similarly, SSMs capture certain frequencies through their learned kernel matrix  $\bar{\mathbf{K}}$  (detailed in Section 3.1). The following equation further illustrates its connection to CNNs:

$$S(t) = (\mathbf{I} \circledast \mathbf{W})(t), \quad (9)$$

where  $\mathbf{W}$  denotes the trainable kernel of the CNN,  $\mathbf{I}$  is the input sequence, and  $S(t)$  is the output at time step  $t$ . When sinusoidal perturbations are introduced, the model’s band-pass characteristics se-

lectively amplify those frequency components, causing it to increasingly attend to the perturbed frequency band and thereby enhancing the effectiveness of BadVim.

While SSMs share convolutional similarities with CNNs, recent studies [4] reveal that SSMs (e.g., Mamba) are limited in their ability to approximate arbitrary continuous input functions, leading to reduced expressivity. This constraint makes them prone to aligning with dominant input patterns—particularly periodic ones introduced by low-rank perturbations. As a result, SSMs tend to more aggressively amplify or suppress specific frequency components, reinforcing the effect of structured signals. Moreover, since Mamba updates its state based on input, the transition matrix  $\bar{\mathbf{A}}$  often aligns with the perturbation frequency. This alignment propagates through the parameters  $\bar{\mathbf{B}}$  and  $\mathbf{C}$ , leading to deviations from the model’s expected behavior. Since  $\bar{\mathbf{K}}$  encodes information from all these parameters, these cumulative effects shape the model’s operation, consistent with the convolutional form.

Building on the above analysis, we observe that periodic perturbations introduced during training induce a frequency-dependent bias in the model’s parameters. This makes the model more sensitive to backdoor triggers operating within the same frequency band. Furthermore, our analysis of the SSM’s state dynamics reveals that such perturbations persist throughout the state transitions, which we refer to as perturbation persistence, as formalized below.

**Proposition 1** (Perturbation Persistence). *Consider the discrete state-space model:  $h_t = \bar{\mathbf{A}}h_{t-1} + \bar{\mathbf{B}}x_t$ ,  $y_t = \mathbf{C}h_t$ . Suppose that the input is corrupted by a low-rank perturbation  $\delta$ , i.e.,  $\hat{x}_t = x_t + \delta$ . Let  $\bar{\mathbf{A}}'$  denote the effective state transition matrix after perturbation. Then, the matrix  $\bar{\mathbf{A}}$  has spectral radius  $\rho(\bar{\mathbf{A}}) > 1$ , the perturbation persists in the state evolution, leading to a spectral radius  $\rho(\bar{\mathbf{A}}') \geq 1$ .*

Specifically, under the conditions on  $\bar{\mathbf{A}}'$ , this persistence leads to a spectral radius  $\rho(\bar{\mathbf{A}}') \geq 1$ , indicating that the perturbation exerts a lasting influence on the model’s behavior and amplifies the backdoor effect. This result supports the intuition that frequency-aligned perturbations persist through state transitions and accumulate in the hidden state over time, rather than dissipating. We provide a detailed proof in the full version of the paper.

## 5 Experiments

### 5.1 Evaluation Settings

**Datasets and Models.** Three common datasets, including CIFAR10 [23], GTSRB [43], and ImageNet [7], were selected for the backdoor poisoning attack. For the VSSM, we adopted Vim-t [58], the tiny-size variant of Vim, which employs bidirectional scanning, the simplest form of VSSM, while other variants use more complex scanning methods. Additionally, we compared robustness across three architectures, including ResNet18 [19], DeiT-t [46]. Since pre-trained models are only available for ImageNet, we trained these models from scratch on CIFAR-10 and GTSRB. Due to space constraints, details on datasets, model architectures, and hyperparameters are provided in the full version.

**Attack Settings.** We utilize a *checkerboard* pattern as the backdoor trigger for our main results. By default, we set the perturbation frequency to 8 and the image-blending ratio to 0.2 for generating poisoning data. Our method was compared with the SOTA backdoor attacks (i.e., BadNets [16], Blend [3], SIG [2], Refool [29], TaCT [45], ISSBA [26], Dynamic [34], WaNet [35], and Adaptive-based [38]),

**Table 1:** The clean accuracy (ACC %) and the attack success rate (ASR %) of three models against backdoor attacks across three datasets, including CIFAR-10, GTSRB and ImageNet. The best results are bolded. The second-best results are underlined. Note that model names marked with “t” denote tiny size.

| Dataset  | Attack    | ResNet18     |              | DeiT-t       |              | Vim-t        |              |
|----------|-----------|--------------|--------------|--------------|--------------|--------------|--------------|
|          |           | ACC          | ASR          | ACC          | ASR          | ACC          | ASR          |
| CIFAR-10 | None      | 94.90        | -            | 90.95        | -            | 86.19        | -            |
|          | BadNets   | 94.08        | <b>100</b>   | <u>90.60</u> | 40.83        | 85.02        | 2.65         |
|          | Blend     | <b>94.21</b> | 92.45        | 90.36        | 96.52        | 85.23        | 88.01        |
|          | SIG       | <u>94.11</u> | 57.68        | 90.42        | 68.26        | 85.43        | 54.27        |
|          | Refool    | 93.17        | 16.43        | 90.51        | 4.17         | 85.52        | 13.48        |
|          | TaCT      | 93.93        | 99.37        | 90.02        | 20.22        | 85.55        | 37.14        |
|          | CLB       | 93.95        | <u>99.90</u> | <b>90.63</b> | 54.19        | 83.47        | 13.27        |
|          | Dynamic   | 93.91        | 98.81        | 90.53        | <u>99.05</u> | <u>85.58</u> | <u>89.75</u> |
|          | ISSBA     | 93.90        | 0.06         | 90.53        | 1.12         | 83.08        | 1.97         |
|          | WaNet     | 93.23        | 1.62         | 89.98        | 1.39         | 84.73        | 2.11         |
|          | Adv-Patch | 93.73        | 99.12        | 90.28        | 3.00         | 85.07        | 7.89         |
|          | Adv-Blend | 93.76        | 51.31        | 90.33        | 38.12        | 85.06        | 56.70        |
|          | Ours      | 93.53        | <b>100</b>   | <b>90.63</b> | <b>100</b>   | <b>85.61</b> | <b>100</b>   |
| GTSRB    | Average   | 93.79        | 68.47        | 90.44        | 43.32        | 84.97        | 38.27        |
|          | None      | 97.22        | -            | 94.10        | -            | 91.27        | -            |
|          | BadNets   | <b>97.19</b> | 1.79         | 92.91        | 77.25        | 92.09        | 1.02         |
|          | Blend     | <u>96.79</u> | <u>92.24</u> | <u>93.17</u> | <u>96.74</u> | <u>92.18</u> | <u>93.70</u> |
|          | SIG       | 96.97        | 44.17        | <u>92.75</u> | 45.40        | 92.07        | 43.73        |
|          | Refool    | 96.71        | 32.56        | 93.09        | 26.83        | 91.96        | 28.15        |
|          | TaCT      | 97.08        | <b>100</b>   | 93.04        | 8.32         | 92.38        | 8.24         |
|          | Dynamic   | 97.00        | <b>100</b>   | 92.79        | <u>99.55</u> | 92.50        | 60.28        |
|          | ISSBA     | 97.03        | 0.11         | 92.81        | 2.21         | <u>92.71</u> | 3.86         |
|          | WaNet     | 96.91        | 0.18         | 92.49        | 0.44         | <u>92.31</u> | 1.08         |
|          | Adv-Patch | <u>97.14</u> | 21.73        | 92.75        | 1.63         | 92.23        | 4.75         |
|          | Adv-Blend | 96.66        | 78.02        | 92.89        | 74.86        | 92.45        | 81.84        |
|          | Ours      | 96.72        | <b>100</b>   | <b>93.51</b> | <b>100</b>   | <b>93.64</b> | <b>100</b>   |
| ImageNet | Average   | 96.92        | 52.26        | 92.92        | 48.56        | 92.35        | 38.06        |
|          | None      | 69.75        | -            | 70.07        | -            | 77.29        | -            |
|          | BadNets   | 69.21        | 75.86        | <u>69.79</u> | <u>95.54</u> | <u>76.75</u> | <u>97.16</u> |
|          | Blend     | <u>69.24</u> | <u>98.58</u> | 68.62        | 92.23        | 76.43        | 86.41        |
|          | Ours      | <b>69.67</b> | <b>99.24</b> | <b>69.85</b> | <b>99.37</b> | <b>77.11</b> | <b>97.89</b> |
|          | Average   | 69.37        | 91.26        | 69.42        | 95.71        | 76.76        | 93.82        |

following the default configuration in Backdoor-ToolBox [38] for fair comparison. The poisoning rate was fixed at 0.3% for all attacks, except for ImageNet, where a higher rate of 1% was used. Additionally, since Backdoor-ToolBox does not implement the clean-label attack (CLB) [48] on GTSRB, we excluded this attack from GTSRB experiments. Further details are provided in our full paper.

**Performance metrics.** We used two common metrics to measure the effectiveness of backdoor attacks: Clean Accuracy (ACC) and Attack Success Rate (ASR). ACC measures the model’s accuracy on benign test data without a backdoor trigger, while ASR evaluates the model’s accuracy when tested on non-target class data with the specified trigger. Generally, a lower ASR coupled with a higher ACC indicates robustness to such attacks.

## 5.2 Empirical Results

**Negligible impact on clean accuracy.** Table 1 presents a comprehensive comparison between the VSSM and the other two models. “None” represents the benign model without backdoor attacks. As can be seen, most models retain competitive ACC on clean samples when subjected to backdoor attacks. Specifically, our attacks on the Vim-t reduce ACC by less than 1%, demonstrating superior performance across three datasets compared to other attacks. Interestingly, we find that Dynamic attack achieves the second-best ACC in CIFAR and GTSRB. We speculate that this is due to its ability to adapt to varying input patterns, which may enhance robustness against perturbations.

Compared to ResNet18 and DeiT-t, Vim-t exhibits a lower average ACC on small-size datasets, *e.g.*, 84.97% on CIFAR10, while it achieves the highest ACC on ImageNet (*i.e.*, 76.76%). This indi-

cates that VSSM benefits from its ability to model long-range dependencies through its state-space representation. Furthermore, we observe that our attacks maintain high ACC across all three models on ImageNet, indicating that the models generalize well to large-scale datasets, with minimal degradation in clean accuracy.

**High attack success rate (ASR).** In Table 1, we observe that Vim-t exhibits lower ASR for most invisible backdoors (*e.g.*, 13.48% and 2.11% in Refool and WaNet on CIFAR10, respectively) compared to visible backdoors. Patch-based triggers, such as BadNets and TaCT, are less effective against Vim-t on small datasets due to the smaller patch size in VSSM, where the trigger is placed at a specific location, causing it to fragment or be disrupted when the image is divided into patches. Vim-t is particularly vulnerable to blending-based and input-aware (*i.e.*, Dynamic) backdoors. This is because SSMs excel at establishing causal correlations between the patches and processing long-sequence inputs, facilitating the synthesis of global triggers. Furthermore, our attacks achieve high ASR across three datasets, *e.g.*, 97.89% on ImageNet, demonstrating their effectiveness on VSSMs.

In comparison with different models, we show that the backdoor robustness of Vim-t is comparable to that of DeiT-t and superior to ResNet18. For instance, on CIFAR10, the average ASR for DeiT-t and Vim-t is 43.32% and 38.27%, respectively, while ResNet18 has an average ASR of 68.47%. Interestingly, our attack successfully injects backdoors into these models (*i.e.*, at higher ASRs). These observations further validate that our attack could transfer to other model architectures. Moreover, this transferability extends across different model architectures, as evidenced by the VSSM’s susceptibility to the attack. Additionally, these results emphasize the backdoor robustness of VSSM, suggesting that while state scanning in SSMs

**Table 2:** Efficacy of model-agnostic defenses against our BadVim.

| Dataset  | No Defense |       | PatchDrop |       | PatchShuffle |       | FT    |       | FP    |       | FT-SAM |       |
|----------|------------|-------|-----------|-------|--------------|-------|-------|-------|-------|-------|--------|-------|
|          | ACC        | ASR   | ACC       | ASR   | ACC          | ASR   | ACC   | ASR   | ACC   | ASR   | ACC    | ASR   |
| CIFAR-10 | 85.60      | 100   | 81.83     | 100   | 69.26        | 100   | 88.86 | 99.97 | 88.71 | 99.97 | 87.46  | 99.94 |
| GTSRB    | 92.42      | 99.90 | 91.95     | 100   | 52.18        | 99.20 | 98.93 | 99.91 | 98.84 | 99.94 | 99.33  | 97.15 |
| ImageNet | 77.11      | 97.89 | 76.44     | 94.06 | 65.93        | 93.14 | 75.48 | 69.83 | 68.46 | 52.96 | 67.80  | 24.32 |

enhances ACC, it remains vulnerable to such attacks.

### 5.3 Resistance to Backdoor Defenses

Due to space limitations, we examine the performance of five existing backdoor defenses and two input-level detection methods against our attack here. We defer a detailed discussion to our full paper.

(1.) PatchDrop [33] and PatchShuffle [22], two patch-processing defense methods for ViTs [8], do not perform as well to eliminate BadVim. As shown in Table 2, the VSSM retains a high ASR (*e.g.*, 94.06% on PatchDrop) under our trigger pattern, while ACC drops significantly (*e.g.*, 65.93% on PatchShuffle) due to the disruption of spatial information.

(2.) Fine-tuning (FT) and fine-pruning (FP) [28] exhibit high ASR in our attack, even with extra clean data (*i.e.*, 5% of the training set). From Table 2, we find that the backdoor behavior is pronounced in small-scale datasets (*e.g.*, 99.97% ASR on CIFAR-10), and although reduced on ImageNet (to 28.06% for FT and 44.93% for FP), this still does not eradicate backdoors.

(3.) Fine-tuning with sharpness-aware minimization (FT-SAM) [59] is the most effective defense among those we evaluated. On ImageNet, it considerably reduces ASR to 24.32%, but performs poorly on CIFAR-10 and GTSRB (*e.g.*, 97.15% ASR). Thus, FT-SAM is ineffective in fully cleansing the backdoored model.

(4.) Strip [12] and cognitive distillation (CD) [20], which focus on input-level backdoor detection, fail to achieve higher TPR and lower FPR on both datasets; the model would still retain backdoors after training, as shown in Table 3. This is because BadVim introduces only an imperceptible perturbation in the spatial domain, making it difficult to identify the backdoor samples.

**Table 3:** Efficacy of input-level backdoor detections against BadVim.

| Dataset | Strip |      |        | CD    |       |        |
|---------|-------|------|--------|-------|-------|--------|
|         | TPR   | FPR  | AUC    | TPR   | FPR   | AUC    |
| CIFAR10 | 33.20 | 9.92 | 0.6766 | 80.39 | 15.73 | 0.8233 |
| GTSRB   | 1.71  | 9.86 | 0.3578 | 19.47 | 13.40 | 0.6122 |

### 5.4 Interpretability of VSSM via Heatmaps

To better understand how SSMs in the VSSM extract image representations, we leverage implicit attention matrices [1] within the SSM layer to analyze and interpret the behavior of backdoored models. As shown in Figure 4, we observe that patch-based methods, such as BadNets, do not shift attention from the object to the trigger; instead, attention is diminished on the object and shifts to edges. This suggests that the backdoor in VSSM arises from the dirty label rather than the trigger pattern. In addition, we find that this phenomenon also occurs in Blend, which can be easily distinguished from benign samples due to its distinct behavior. In contrast, the heat maps generated from our attacks are similar to those of the clean and backdoor images. This is because the image is generated by adding an extremely small perturbation to the clean image; thus, the difference in the hidden attention, where the heat maps are generated, is also minimal. Consequently, existing defense methods [44] that detect backdoors based on trigger-induced attention shifts in heatmaps

fail to distinguish our backdoor samples from clean ones, rendering them ineffective against our attack.

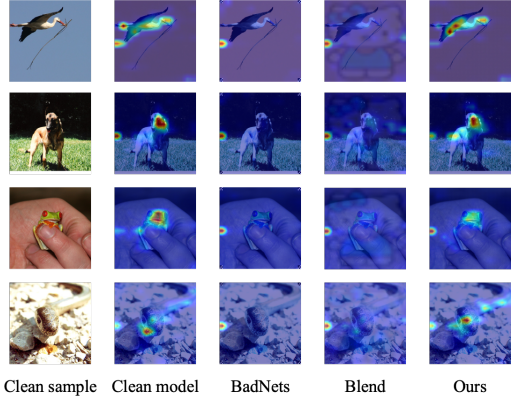


**Figure 4:** Visualization of VSSM under implicit attention matrices [1] on ImageNet. We evaluate clean samples using the clean model (second column) and poisoned samples using the backdoored model (third to fifth columns), respectively.

### 5.5 Robustness Analysis: Architecture and Model Scale

**Evaluation of BadVim on Different VSSMs.** We evaluate the effectiveness of BadVim on another VSSM, VMamba [30], which differs from Vim in its scanning trajectory and architectural modules. As shown in Table 4, VMamba-t achieves a notably higher ASR under our attack (*i.e.*, 99.98%) than Vim-t, while maintaining high ACC. Compared to Vim-t, VMamba-t demonstrates stronger robustness against BadNets and Blend, achieving lower ASR values (*i.e.*, 41.92% and 26.16%). These findings suggest that BadVim effectively exploits the sequential state processing patterns and inductive biases inherent to these models. Thus, both VSSMs are susceptible to BadVim, revealing a shared vulnerability within the model.

**Table 4:** Comparison between Vim and VMamba under Backdoor Attacks on ImageNet.

| Attacks Type | BadNets |              | Blend        |              | Ours  |              |              |
|--------------|---------|--------------|--------------|--------------|-------|--------------|--------------|
| Model        | ACC     | ASR          | ACC          | ASR          | ACC   | ASR          |              |
| Vim-t        | 77.29   | <u>76.75</u> | <u>97.16</u> | 76.43        | 86.41 | <b>77.11</b> | <b>97.89</b> |
| VMamba-t     | 81.84   | 81.51        | <u>41.92</u> | <u>81.55</u> | 26.16 | <b>81.88</b> | <b>99.98</b> |

**VSSM vs. Gated CNN.** In Table 5, we compare the backdoor robustness of VSSMs and Gated CNNs, which differ only in the use of the SSM mechanism. We fine-tuned Vim-t [58] and GatedCNN-t [53] for ten epochs. Vim-t shows high ASR under BadNets and Blend (up to 99.16%) but with a moderate drop in ACC (down to 75.06%). In contrast, GatedCNN-t achieves lower ASR (*e.g.*, 35.30%) while retaining similar ACC (*e.g.*, 78.51%), suggesting stronger robustness due to its ability to capture global patterns and semantic features across entire images through well-designed convolutional layers.

Our method maintains competitive ASR on both architectures (*e.g.*, 97.89% on Vim-t and 98.32% on GatedCNN-t) with minimal

**Table 5:** Comparison of VSSMs and Gated CNNs under Backdoor Attacks on ImageNet.

| Attacks Type |       | BadNets |       | Blend |       | Ours  |       |
|--------------|-------|---------|-------|-------|-------|-------|-------|
| Model        | ACC   | ACC     | ASR   | ACC   | ASR   | ACC   | ASR   |
| Vim-t        | 77.29 | 76.75   | 97.16 | 76.43 | 86.41 | 77.11 | 97.89 |
| GatedCNN-t   | 78.77 | 78.51   | 35.30 | 78.71 | 73.34 | 78.68 | 98.32 |

ACC degradation. This is attributed to VSSM’s emphasis on local features, as it processes images patch (state) by patch (state) to model long-range dependencies. These results demonstrate that BadVim, based on the low-rank perturbation, delivers consistent effectiveness across architectures. Detailed analysis is provided in our full version.

## 5.6 Ablation Studies

**Impact of Model Size on Backdoor Robustness.** In Table 6, we analyze the influence of different model sizes on the VSSM against backdoor robustness. We evaluated three pre-trained models from Vim, where our attack consistently achieves a high ASR, reaching 97.89% on Vim-t, while maintaining high accuracy (*i.e.*, 77.11%), compared to BadNets and Blend. As the model size increases, Vim-s shows a slight decrease in ASR, reaching 82.35% for BadNets and 82.76% for Blend. Vim-b reduces the impact of backdoor trigger features by distributing the learned information across more dimensions. This makes it harder for the attacker to exploit the specific trigger to induce backdoor behavior in the target model, improving its robustness against backdoor attacks.

**Table 6:** Backdoor robustness evaluation on different sizes of VSSM with ImageNet. Model names marked with “t” denote tiny size, “s” small size, and “b” base size.

| Attack | BadNets |       | Blend |       | Ours  |       |       |
|--------|---------|-------|-------|-------|-------|-------|-------|
| Model  | ACC     | ACC   | ASR   | ACC   | ASR   | ACC   | ASR   |
| Vim-t  | 77.29   | 76.75 | 97.16 | 76.43 | 86.41 | 77.11 | 97.89 |
| Vim-s  | 81.08   | 80.98 | 82.35 | 81.10 | 82.76 | 81.02 | 83.50 |
| Vim-b  | 80.13   | 79.51 | 72.92 | 79.70 | 28.50 | 79.84 | 74.67 |

**Effect of Poisoning Rate on ASR.** We explore the impact of different poisoning rates on Vim-t by fine-tuning the pre-trained model. As shown in Figure 5, both BadNets and Blend achieve high ASR at poisoning rates as low as 1%. However, at a poisoning rate of 0.3%, ASR drops significantly for both attacks, *i.e.*, 40.22% for BadNets and 75.92% for Blend, indicating that the backdoor attack becomes less effective. In contrast, our proposed trigger maintains a high ASR of 88.14% even at an extremely low poisoning rate of 0.3%, showcasing its effectiveness against the VSSM.

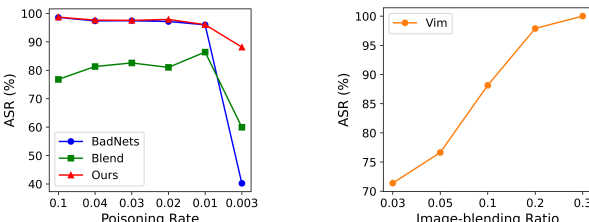


**Figure 5:** Effect of poisoning rate. **Figure 6:** Effect of blending rate.

**Effect of Blending Rate on ASR.** We examine the effect of varying blending ratios on Vim-t by fine-tuning the pre-trained model. As shown in Figure 6, ASR increases with higher blending ratios. We select a fixed blending ratio of 0.2 to balance attack effectiveness and

trigger stealthiness. Importantly, even at a low blending ratio of 0.03, the ASR still exceeds 70%. This indicates that even slight perturbations are sufficient for the model to memorize the pattern, demonstrating the efficacy of BadVim against VSSMs.

## 6 Discussion and limitations

### 6.1 Backdoor Robustness: VSSMs vs. ViTs

Recent studies (*e.g.*, [17]) suggest that the VSSM block can be viewed as a variant of linear attention, incorporating an input gate and a forget gate (*i.e.*,  $\bar{A}$  in Equation 2). While these modifications improve task performance, the recurrent computation of the forget gate may be suboptimal for vision models. Moreover, as shown in Section 5.2, linear attention-like mechanisms do not enhance backdoor robustness and are more vulnerable to certain triggers (*e.g.*, patch-based and image-blend). Given structural similarities between ViTs and VSSMs—particularly their reliance on patch tokenization and linear projections—we conclude that their backdoor robustness is likely comparable as well.

### 6.2 Adversarial vs. Backdoor Robustness in VSSMs

Following the previous work [50] that highlights a trade-off between adversarial and backdoor robustness, such a similar phenomenon is also observed in the VSSM. Specifically, the study [10] indicates that the VSSM is more robust to adversarial attacks than ViTs due to the challenging gradient estimation. The trade-off between model size and robustness becomes more apparent as model size increases. In contrast, our findings reveal that *the backdoor robustness of the VSSM is comparable to that of ViTs but slightly lower than that of GatedCNNs without SSM modules*. These results suggest that future research should consider backdoor robustness when developing novel architectures or defenses to mitigate potential threats.

### 6.3 Limitations

We discuss the robustness of SSM mechanism in the VSSMs against backdoor attacks in this work. However, we cannot delve into the impact of SSM parameters on backdoors, as tracking and accessing these parameters during training remains challenging. Moreover, our trigger pattern for VSSM is based on patch sensitivity analysis, which may not necessarily be optimal. Finally, while our focus has been on the SSM mechanism of VSSM in image classification tasks, this mechanism has also been applied to other domains, such as natural language processing. We consider extending the research to these domains as part of our ongoing work.

## 7 Conclusions

In this paper, we present a systematic study of the vulnerability of VSSMs to backdoor attacks, which exploit the state-space representation inherent in SSMs. Building on this insight, we propose BadVim, a low-rank perturbation approach that subtly disturbs key parameters in SSMs to implant backdoors. Specifically, we introduce three imperceptible periodic patterns as triggers and embed them into benign samples to generate poisoned samples. Our experiments show that BadVim is effective and successfully evades existing defenses, with hidden attention matrices resembling those of clean samples. We hope that our findings will inform the development of more robust defense strategies for VSSMs.

## Acknowledgements

This work was supported by the National Science and Technology Council (NSTC) with Grant NSTC 112-2221-E-001-011-MY2 and Academia Sinica with Grant AS-IAIA-114-M08.

## References

- [1] A. Ali, I. Zimerman, and L. Wolf. The hidden attention of mamba models. *arXiv preprint arXiv:2403.01590*, 2024.
- [2] M. Barni, K. Kallas, and B. Tondi. A new backdoor attack in cnns by training set corruption without label poisoning. In *IEEE ICIP*, pages 101–105. IEEE, 2019.
- [3] X. Chen, C. Liu, B. Li, K. Lu, and D. Song. Targeted backdoor attacks on deep learning systems using data poisoning. *arXiv preprint arXiv:1712.05526*, 2017.
- [4] N. M. Cirone, A. Orvieto, B. Walker, C. Salvi, and T. Lyons. Theoretical foundations of deep selective state-space models. In *NIPS*, 2024.
- [5] K. L. Clarkson and D. P. Woodruff. Low-rank approximation and regression in input sparsity time. *Journal of ACM*, 63(6):1–45, 2017.
- [6] T. Dao and A. Gu. Transformers are SSMs: Generalized models and efficient algorithms through structured state space duality. In *ICML*, 2024.
- [7] J. Deng, W. Dong, R. Socher, L.-J. Li, K. Li, and L. Fei-Fei. Imagenet: A large-scale hierarchical image database. In *CVPR*, pages 248–255, 2009.
- [8] K. D. Doan, Y. Lao, P. Yang, and P. Li. Defending backdoor attacks on vision transformer via patch processing. In *AAAI*, 2023.
- [9] A. Dosovitskiy, L. Beyer, A. Kolesnikov, D. Weissenborn, X. Zhai, T. Unterthiner, M. Dehghani, M. Minderer, G. Heigold, S. Gelly, J. Uszkoreit, and N. Houlsby. An image is worth 16x16 words: Transformers for image recognition at scale. In *ICLR*, 2021.
- [10] C. Du, Y. Li, and C. Xu. Understanding robustness of visual state space models for image classification. *arXiv preprint arXiv:2403.10935*, 2024.
- [11] D. Y. Fu, T. Dao, K. K. Saab, A. W. Thomas, A. Rudra, and C. Re. Hungry hungry hippos: Towards language modeling with state space models. In *ICLR*, 2023.
- [12] Y. Gao, C. Xu, D. Wang, S. Chen, D. C. Ranasinghe, and S. Nepal. Strip: A defence against trojan attacks on deep neural networks. In *ACSAC*, pages 113–125, 2019.
- [13] A. Gu and T. Dao. Mamba: Linear-time sequence modeling with selective state spaces. In *COLM*, 2024.
- [14] A. Gu, T. Dao, S. Ermon, A. Rudra, and C. Ré. Hippo: Recurrent memory with optimal polynomial projections. *NIPS*, 33:1474–1487, 2020.
- [15] A. Gu, K. Goel, and C. Re. Efficiently modeling long sequences with structured state spaces. In *ICLR*, 2022.
- [16] T. Gu, K. Liu, B. Dolan-Gavitt, and S. Garg. Badnets: Evaluating backdooring attacks on deep neural networks. *IEEE Access*, 7:47230–47244, 2019.
- [17] D. Han, Z. Wang, Z. Xia, Y. Han, Y. Pu, C. Ge, J. Song, S. Song, B. Zheng, and G. Huang. Demystify mamba in vision: A linear attention perspective. In *NIPS*, 2024.
- [18] A. Hatamizadeh and J. Kautz. Mambavision: A hybrid mamba-transformer vision backbone. In *CVPR*, 2025.
- [19] K. He, X. Zhang, S. Ren, and J. Sun. Deep residual learning for image recognition. In *CVPR*, pages 770–778, 2016.
- [20] H. Huang, X. Ma, S. M. Erfani, and J. Bailey. Distilling cognitive backdoor patterns within an image. In *ICLR*, 2023.
- [21] K. Huang, Y. Li, B. Wu, Z. Qin, and K. Ren. Backdoor defense via decoupling the training process. In *ICLR*, 2022.
- [22] G. Kang, X. Dong, L. Zheng, and Y. Yang. Patchshuffle regularization. *arXiv preprint arXiv:1707.07103*, 2017.
- [23] A. Krizhevsky, G. Hinton, et al. Learning multiple layers of features from tiny images. *Technical report, Univ. of Toronto*, 2009.
- [24] S. Li, M. Xue, B. Z. H. Zhao, H. Zhu, and X. Zhang. Invisible backdoor attacks on deep neural networks via steganography and regularization. *IEEE TDSC*, 18(5):2088–2105, 2020.
- [25] S. Li, H. Singh, and A. Grover. Mamba-nd: Selective state space modeling for multi-dimensional data. In *ECCV*, pages 75–92. Springer, 2024.
- [26] Y. Li, Y. Li, B. Wu, L. Li, R. He, and S. Lyu. Invisible backdoor attack with sample-specific triggers. In *ICCV*, pages 16463–16472, 2021.
- [27] Y. Li, Y. Jiang, Z. Li, and S.-T. Xia. Backdoor learning: A survey. *IEEE TNNLS*, 35(1):5–22, 2022.
- [28] K. Liu, B. Dolan-Gavitt, and S. Garg. Fine-pruning: Defending against backdooring attacks on deep neural networks. In *RAID*, pages 273–294. Springer, 2018.
- [29] Y. Liu, X. Ma, J. Bailey, and F. Lu. Reflection backdoor: A natural backdoor attack on deep neural networks. In *ECCV*, pages 182–199. Springer, 2020.
- [30] Y. Liu, Y. Tian, Y. Zhao, H. Yu, L. Xie, Y. Wang, Q. Ye, J. Jiao, and Y. Liu. VMamba: Visual state space model. In *NIPS*, 2024.
- [31] Z. Liu, H. Mao, C.-Y. Wu, C. Feichtenhofer, T. Darrell, and S. Xie. A convnet for the 2020s. In *CVPR*, pages 11976–11986, 2022.
- [32] H. Mehta, A. Gupta, A. Cutkosky, and B. Neyshabur. Long range language modeling via gated state spaces. In *ICLR*, 2023.
- [33] M. M. Naseer, K. Ranasinghe, S. H. Khan, M. Hayat, F. Shahbaz Khan, and M.-H. Yang. Intriguing properties of vision transformers. *NIPS*, 34:23296–23308, 2021.
- [34] T. A. Nguyen and A. Tran. Input-aware dynamic backdoor attack. *NIPS*, 33:3454–3464, 2020.
- [35] T. A. Nguyen and A. T. Tran. Wanet - imperceptible warping-based backdoor attack. In *ICLR*, 2021.
- [36] N. Papernot, P. McDaniel, S. Jha, M. Fredrikson, Z. B. Celik, and A. Swami. The limitations of deep learning in adversarial settings. In *IEEE EuroS&P*, pages 372–387. IEEE, 2016.
- [37] B. Qi, Y. Luo, J. Gao, P. Li, K. Tian, Z. Ma, and B. Zhou. Exploring adversarial robustness of deep state space models. In *NIPS*, 2024.
- [38] X. Qi, T. Xie, Y. Li, S. Mahloojifar, and P. Mittal. Revisiting the assumption of latent separability for backdoor defenses. In *ICLR*, 2023.
- [39] H. Qiu, H. Ma, Z. Zhang, A. Abuadba, W. Kang, A. Fu, and Y. Gao. Towards a critical evaluation of robustness for deep learning backdoor countermeasures. *IEEE TIFS*, 19:455–468, 2023.
- [40] M. Ravanelli and Y. Bengio. Speaker recognition from raw waveform with sincnet. In *IEEE spoken language technology workshop (SLT)*, pages 1021–1028. IEEE, 2018.
- [41] V. Shejwalkar, L. Lyu, and A. Houmansadr. The perils of learning from unlabeled data: Backdoor attacks on semi-supervised learning. In *ICCV*, pages 4730–4740, 2023.
- [42] J. T. Smith, A. Warrington, and S. Linderman. Simplified state space layers for sequence modeling. In *ICLR*, 2023.
- [43] J. Stallkamp, M. Schlippling, J. Salmen, and C. Igel. The german traffic sign recognition benchmark: a multi-class classification competition. In *IJCNN*, pages 1453–1460, 2011.
- [44] A. Subramanya, S. A. Koohpayegani, A. Saha, A. Tejankar, and H. Pirsiavash. A closer look at robustness of vision transformers to backdoor attacks. In *WACV*, pages 3874–3883, 2024.
- [45] D. Tang, X. Wang, H. Tang, and K. Zhang. Demon in the variant: Statistical analysis of {DNNs} for robust backdoor contamination detection. In *USENIX*, pages 1541–1558, 2021.
- [46] H. Touvron, M. Cord, M. Douze, F. Massa, A. Sablayrolles, and H. Jégou. Training data-efficient image transformers & distillation through attention. In *ICML*, pages 10347–10357, 2021.
- [47] H. Touvron, P. Bojanowski, M. Caron, M. Cord, A. El-Nouby, E. Grave, G. Izacard, A. Joulin, G. Synnaeve, J. Verbeek, et al. Resmlp: Feed-forward networks for image classification with data-efficient training. *IEEE TPAMI*, 45(4):5314–5321, 2022.
- [48] A. Turner, D. Tsipras, and A. Madry. Label-consistent backdoor attacks. *arXiv preprint arXiv:1912.02771*, 2019.
- [49] J. Wang, D. Paliotta, A. May, A. M. Rush, and T. Dao. The mamba in the llama: Distilling and accelerating hybrid models. In *NIPS*, 2024.
- [50] C.-H. Weng, Y.-T. Lee, and S.-H. B. Wu. On the trade-off between adversarial and backdoor robustness. *NIPS*, 33:11973–11983, 2020.
- [51] H. Wu, Y. Yang, H. Xu, W. Wang, J. Zhou, and L. Zhu. Rainmamba: Enhanced locality learning with state space models for video deraining. In *ACM MM*, 2024.
- [52] Z. Xing, T. Ye, Y. Yang, G. Liu, and L. Zhu. Segmamba: Long-range sequential modeling mamba for 3d medical image segmentation. In *MICCAI*, 2024.
- [53] W. Yu and X. Wang. Mambabout: Do we really need mamba for vision? In *CVPR*, 2025.
- [54] W. Yu, P. Zhou, S. Yan, and X. Wang. Inceptionnext: When inception meets convnext. In *CVPR*, pages 5672–5683, 2024.
- [55] Z. Yuan, P. Zhou, K. Zou, and Y. Cheng. You are catching my attention: Are vision transformers bad learners under backdoor attacks? In *CVPR*, pages 24605–24615, 2023.
- [56] G. Zhang, L. Fan, C. He, Z. Lei, Z. Zhang, and L. Zhang. Voxel mamba: Group-free state space models for point cloud based 3d object detection. In *NIPS*, 2024.
- [57] Z. Zhao, X. Chen, Y. Xuan, Y. Dong, D. Wang, and K. Liang. Defeat: Deep hidden feature backdoor attacks by imperceptible perturbation and latent representation constraints. In *CVPR*, pages 15213–15222, 2022.
- [58] L. Zhu, B. Liao, Q. Zhang, X. Wang, W. Liu, and X. Wang. Vision mamba: Efficient visual representation learning with bidirectional state space model. In *ICML*, 2024.

- [59] M. Zhu, S. Wei, L. Shen, Y. Fan, and B. Wu. Enhancing fine-tuning based backdoor defense with sharpness-aware minimization. In *ICCV*, pages 4466–4477, 2023.
- [60] M. Zhu, S. Wei, H. Zha, and B. Wu. Neural polarizer: A lightweight and effective backdoor defense via purifying poisoned features. *NIPS*, 36, 2024.

The content of Supplementary Material is organized as follows: (1) Section 8 reviews the State Space Model (SSM) paradigm to explain its application in VSSMs; (2) Section 9 and 10 describe the BadVim algorithms in detail and provide analytical evidence to elucidate their impact on VSSMs; (3) Section 11 presents the implementation and training details, including datasets, hyperparameters, and attack settings, to ensure the reproducibility of our work; (4) Section 12 and 13 provide additional experimental results and discuss the differences between Gated CNNs and VSSMs.

## 8 Revisit the concept of S4

We first define the HiPPO matrix [14], which specifies a class of matrices  $\mathbf{A} \in \mathbb{R}^{N \times N}$  that, when incorporated into Equation 1, enables the state  $x(t)$  to retain the history of the input  $u(t)$ . The HiPPO matrix is given by

$$\mathbf{A}_{nk} = - \begin{cases} (2n+1)^{1/2}(2k+1)^{1/2}, & \text{if } n > k, \\ n+1, & \text{if } n = k, \\ 0, & \text{if } n < k. \end{cases} \quad (10)$$

A key concept in S4 [15] is the efficient computation of all views of SSMs (Section 3.1). Specifically, S4 establishes an equivalence relation on SSMs:  $(\mathbf{A}, \mathbf{B}, \mathbf{C}) \sim (\mathbf{V}^{-1}\mathbf{A}\mathbf{V}, \mathbf{V}^{-1}\mathbf{B}, \mathbf{C}\mathbf{V})$ . This transformation accelerates computation when  $\mathbf{A}$  is diagonal. Ideally,  $\mathbf{A}$  would be diagonalizable by a unitary matrix, as guaranteed by the Spectral Theorem for normal matrices. However, normality is a restrictive condition that the HiPPO matrix does not satisfy. S4 observes that the HiPPO matrix can be decomposed into normal and low-rank components, though this alone does not enable efficient computation. To address this, S4 introduces three techniques (*i.e.*, Cauchy Kernel, Woodbury Identity, and truncated generating function) to overcome this bottleneck and generalize the Normal Plus Low-Rank (NPLR) decomposition to arbitrary matrices.

**Theorem 2.** All HiPPO matrices from [14] admit an NPLR decomposition of the form

$$\mathbf{A} = \mathbf{V}\Lambda\mathbf{V}^* - \mathbf{P}\mathbf{Q}^T = \mathbf{V}(\Lambda - (\mathbf{V}^*\mathbf{P})(\mathbf{V}^*\mathbf{Q})^T)\mathbf{V}, \quad (11)$$

where  $\mathbf{V} \in \mathbb{C}^{N \times N}$  is unitary,  $\Lambda$  is diagonal, and  $\mathbf{P}, \mathbf{Q} \in \mathbb{R}^{N \times r}$  form a low-rank factorization. The HiPPO matrices LegS, LegT, and LagT satisfy  $r = 1$  or  $r = 2$ . In particular, Equation 10 corresponds to an NPLR decomposition with  $r = 1$ .

We omit variant HiPPO matrices (*i.e.*, LegS, LegT, and LagT) in this paper; please refer to S4 [15] for further details. Here, we note that any VSSM based on low-rank matrix approximation [5] can reduce the time complexity of state updates.

## 9 Details of BadVim

### 9.1 Trigger pattern

In the BadVim framework, we present three strategies for constructing trigger patterns using various frequency- or pixel-based techniques. Notably, embedding the trigger pattern in each patch increases its robustness to perturbations. A straightforward approach is to use a static trigger, such as a single pixel, placed repeatedly across the image [41]. This ensures that the pattern remains spatially consistent and unaffected by geometric transformations. Although similar in form to prior work [41], our method differs in both its goal and application context. Despite the state-sequence updates and patch-wise processing in VSSMs, we find that these embedded triggers can still successfully compromise the model.

## 9.2 Our Algorithms

Our attacks are described in Algorithm 1. Specifically, BadVim enables an adversary to select one of the strategies and inject it into the training data with a predefined poisoning rate. This approach highlights that when applied to each patch, low-rank perturbations can influence VSSMs during state updates and are more effective than SOTA attacks.

---

#### Algorithm 1: Training of BadVim

---

```

1 Input: Training data  $D_{train} = \{(x_i, y_i)\}$ , a loss function
    $\mathcal{L}_{vss}$ , a mapping function  $\mathcal{T}$ , three strategies
    $\mathcal{S} = \{S_1, S_2, S_3\}$ , where  $S_1$  is “Sinusoidal wave,”  $S_2$  is
   “Checkerboard,” and  $S_3$  is “Stripes.” In addition, let  $f_x/f_y$ 
   denote the frequency intensity and  $\alpha$  the blending rate.
2 Output: Backdoored Model  $\mathcal{M}_{bd}$ .
3 /* Step 0: Pick a strategy */ *
4  $S^* \leftarrow \mathcal{S}$ 
5 /*  $D_{train}$  is a training dataset */ *
6 for  $(x_i, y_i) \in D_{train}$  do
7   /* Step 1: Generate BadVim trigger based on
      the selected strategy */ *
8   if  $S^* == S_1$  then
9     /* Generate sinusoidal wave trigger
        (LRP-Sine) */ *
10     $I(x, y) =$ 
11    
$$\sum_k [a_k \sin(2\pi\omega_k x + \phi_k) + b_k \sin(2\pi\omega_k y + \psi_k)]$$

12  else if  $S^* == S_2$  then
13    /* Generate checkerboard trigger
        (LRP-Checkerboard) */ *
14     $I(x, y) = \text{sign}(\sin(2\pi f_x x) \sin(2\pi f_y y))$ 
15  else if  $S^* == S_3$  then
16    /* Generate stripe trigger (LRP-Stripes)
       */ *
17     $I(x, y) = \text{sign}(\sin(2\pi f_x x) + \sin(2\pi f_y y))$ 
18  else
19    /* Step 2: Apply the trigger to the pixel
       domain and blend it with the clean image
       */ *
20     $x'_i = \mathcal{T}(x_i, I(x, y), \alpha)$ 
21  /* Step 3: Update the training dataset with
     the poisoned images */ *
22   $D_{train}^{bd} \leftarrow D_{train} \cup \{x'_i\}$ 
23 /* Train a backdoored model  $\mathcal{M}_{bd}$  on the
   poisoned data */ *
24 Randomly initialize a model  $\mathcal{M}$ 
25  $\mathcal{M}_{bd} = \mathcal{M}(D_{train}^{bd}, \mathcal{L}_{vss})$  return Model  $\mathcal{M}_{bd}$ 

```

---

## 10 Proofs

*Proof of Proposition 1.* We first define the state evolution over multiple time steps under the presence of the perturbation during training and inference.

**Training Formulation.** Consider the training state evolution equation without perturbation:

$$h_t = \bar{\mathbf{A}}h_{t-1} + \bar{\mathbf{B}}x_t.$$

Now, suppose that the training samples are corrupted with a low-rank perturbation  $\delta$ , such that the poisoned input is  $\hat{x}_t = x_t + \delta$ . The

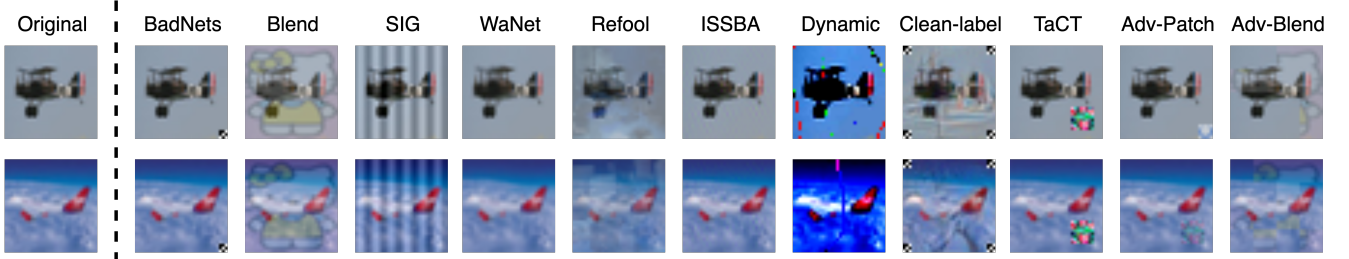


Figure 7: Example images of backdoored samples from CIFAR-10 dataset with 11 attacks.

corresponding state evolution equation becomes:

$$h'_t = \bar{\mathbf{A}}' h'_{t-1} + \bar{\mathbf{B}}' (x_t + \delta),$$

where  $\bar{\mathbf{A}}'$  and  $\bar{\mathbf{B}}'$  denote the model parameters learned under the influence of the perturbation. Since the training data is modified, the learned transition matrix deviates from its clean counterpart:  $\bar{\mathbf{A}}' = \mathbf{A} + E$ ,  $\bar{\mathbf{B}}' = \mathbf{B} + F$ , where  $E$  and  $F$  capture the differences induced by training on perturbed data. Notably, if the perturbation  $\delta$  is low-rank, then  $E$  is also expected to be low-rank due to its dependence on  $\delta$ .

**Propagating the State Evolution.** Expanding the recurrence over  $t$  steps, we obtain:

$$h'_t = \bar{\mathbf{A}}^t h_0 + \sum_{i=0}^{t-1} \bar{\mathbf{A}}^i \bar{\mathbf{B}}' \hat{x}_{t-i}$$

Similarly, under backdoor training:

$$h'_t = \bar{\mathbf{A}}'^t h_0 + \sum_{i=0}^{t-1} \bar{\mathbf{A}}'^i \bar{\mathbf{B}}' \hat{x}_{t-i} + \sum_{i=0}^{t-1} \bar{\mathbf{A}}'^i \bar{\mathbf{B}}' \delta.$$

The term  $S_t = \sum_{i=0}^{t-1} \bar{\mathbf{A}}'^i \bar{\mathbf{B}}' \delta$  captures the cumulative effect of the perturbation across time.

**Spectral Radius Condition.** To understand the long-term behavior of  $S_t$ , we analyze the spectral radius of  $\bar{\mathbf{A}}'$ . Applying standard spectral perturbation bounds:

$$\rho(\bar{\mathbf{A}}') \geq \rho(\bar{\mathbf{A}}) - \|E\|.$$

Since the perturbation matrix  $E$  is low-rank with a small norm, its effect on the spectral radius is negligible unless  $\bar{\mathbf{A}}$  is already near a critical threshold. If  $\rho(\bar{\mathbf{A}}') \geq 1$ , then small perturbations  $E$  are insufficient to ensure contraction, implying  $\rho(\bar{\mathbf{A}}') \geq 1$  in most cases.

We now analyze the two cases:

- **Case 1:**  $\rho(\bar{\mathbf{A}}') = 1$  In this case,  $\bar{\mathbf{A}}'^i$  does not decay. So, the accumulated perturbation  $S_t$  remains significant and persists throughout the state trajectory.
- **Case 2:**  $\rho(\bar{\mathbf{A}}') > 1$  The term  $\bar{\mathbf{A}}'^i$  grows, leading to an unbounded accumulation of the perturbation effect. As a result, the poisoned model's state diverges significantly from the clean model over time.

Since in both cases, the perturbation  $\delta$  does not decay, we conclude that it persists in the model's state evolution. Under the condition  $\rho(\bar{\mathbf{A}}') \geq 1$ , the perturbation's influence remains non-negligible throughout training and inference.  $\square$

## 11 Experimental Settings

**Datasets.** We provide details of the datasets used in our experiments in Table 7, showing the number of classes, training samples, and test samples for each. These datasets [23, 43, 7] are commonly used to evaluate backdoor attacks.

Table 7: Statistics of datasets used in our experiments.

| Dataset  | Input size                | Classes | Training data | Test data |
|----------|---------------------------|---------|---------------|-----------|
| CIFAR10  | $3 \times 32 \times 32$   | 10      | 50,000        | 10,000    |
| GTSRB    | $3 \times 32 \times 32$   | 43      | 39,209        | 12,630    |
| ImageNet | $3 \times 224 \times 224$ | 1000    | 1,281,167     | 100,000   |

**Training Setting.** Following the training settings in Vim [58], we adopt an AdamW optimizer with a momentum of 0.9, a weight decay of  $1 \times 10^{-8}$ , a mixup rate of 0.8, a warmup learning rate of  $1 \times 10^{-5}$ , and an initial learning rate of  $5 \times 10^{-6}$  in our experiments. With a batch size of 128, we fine-tune the pre-trained model on ImageNet for three epochs. Furthermore, we perform the experiments using a single NVIDIA V100 GPU with 32GB RAM, which requires approximately 16 hours for the above experiments. Besides, for CIFAR10 and GTSRB, we set the patch size to 4, the embedding dimension to 256, and the model depth to 12, in contrast to the settings of 16, 192, and 24 used for ImageNet. For DeiT [46] and GatedCNN [53], we follow the original setting in the official code to train models. Since the pre-trained models are only available for ImageNet, we train the models from scratch on CIFAR10 and GTSRB.

**Attacks Setting.** We consider several backdoor attacks and follow the default configuration in Backdoor-Toolbox [38]. The attacks in our experiments have a poisoning rate of 0.3%. Furthermore, since Backdoor-ToolBox does not implement the clean-label attack (CLB) on GTSRB, we do not use this attack on GTSRB. Besides, our trigger pattern focuses on the large-scale dataset, aiming to enhance backdoor effectiveness. Consequently, we have omitted experiments on CIFAR10 and GTSRB. For clarity, we present visualization results of the backdoor attacks used in this paper, as shown in Figure 7, using examples from CIFAR10. These include both visible and invisible types, as well as adaptive attacks [38] such as Adv-Patch and Adv-Blend.

**Defenses Setting.** Since existing defenses are primarily designed for CNN and ViT architectures, we adapt five model-agnostic backdoor defenses: two for patch processing and three for in-training defense.

**(1.) Patch processing defense:** Recall that patch processing techniques [8] effectively disrupt trigger patterns to combat backdoor attacks on ViTs. Specifically, the first approach, PatchDrop [33], randomly removes a certain number of patches from an image, leading to information loss. The second approach, PatchShuffle [22], randomly shuffles the patches within the image's spatial grid. Despite the fact that this method retains the image content, it significantly impacts the receptive fields of the models. To ensure effectiveness,

we set the drop rate as 0.3 in PatchDrop [33] and used the model’s original patch size for PatchShuffle [22], as shown in Figure 8. A higher drop rate and smaller patch size result in more severe disruption of spatial information.

**(2) In-training defense:** We fine-tune with auxiliary clean data (*i.e.*, 5% of training data). FT [28] and FT-SAM [59] are trained for 100 epochs. FT-SAM uses a sharpness-aware optimizer to minimize the loss function, thereby enhancing model generalization by reducing the sharpness of the loss surface, whereas FT applies traditional fine-tuning without such enhancements. For FT, we perform fine-pruning by removing 20% of the weights in the convolutional and linear layers before fine-tuning for 10 epochs.



**Figure 8:** Illustration of patch processing defense. We randomly drop patches or shuffle the patches within the image to disrupt trigger patterns, with a drop rate of 0.3 and patch size of 16 in this sample.

## 12 More Experimental Results

**Different strategies in BadVim.** Table 8 shows that all three BadVim strategies achieve high ASR on CIFAR10 and GTSRB. Notably, the “LRP-Checkerboard” pattern attains 100% ASR on both datasets while maintaining strong ACC values of 85.58% and 93.65%, respectively. In comparison, the “LRP-Sine” and “LRP-Stripes” trigger patterns yield slightly lower ASR and ACC, with the “LRP-Sine” pattern achieving 96.32% ASR on CIFAR10 and 86.48% on GTSRB. These results further corroborate our finding that the state transitions inherent to VSSMs make it prone to backdoor attacks. Therefore, we adopt the “LRP-Checkerboard” pattern for the main results in this paper.

**Table 8:** Backdoor attack performance across three strategies.

| Strategy → | LR-Sine       | LR-Check             | LR-Stripes    |
|------------|---------------|----------------------|---------------|
| Dataset ↓  | ACC   ASR     | ACC   ASR            | ACC   ASR     |
| CIFAR10    | 85.23   96.32 | <b>85.58   100  </b> | 84.88   97.56 |
| GTSRB      | 92.28   86.48 | 93.65   <b>100  </b> | 93.42   98.89 |

**Evaluation of Trigger Pattern Quality.** Table 9 summarizes the image quality after applying different low-rank perturbation (LRP) trigger strategies. Among the three designs, the checkerboard pattern achieves the highest PSNR (*i.e.*, 37.27 on CIFAR10, 37.38 on GTSRB) and SSIM scores (*i.e.*, 0.9893 and 0.9781, respectively), indicating minimal visual distortion when embedding the trigger. In contrast, the sine and stripe patterns yield lower PSNR and SSIM values, reflecting more noticeable perturbations. These results suggest that the “LRP-Checkerboard” trigger achieves a better trade-off between stealthiness and attack effectiveness across both datasets.

**Table 9:** Comparison of image quality with our three strategies on CIFAR10 and GTSRB.

| Strategy         | CIFAR10 |             | GTSRB |             |
|------------------|---------|-------------|-------|-------------|
|                  | PSNR    | SSIM        | PSNR  | SSIM        |
| LRP-Sine         | 34.23   | 0.9652±.026 | 34.26 | 0.9310±.058 |
| LRP-Checkerboard | 37.27   | 0.9893±.009 | 37.38 | 0.9781±.020 |
| LRP-Stripes      | 32.60   | 0.9831±.015 | 32.71 | 0.9645±.033 |

## 13 Distinction between Gated CNNs and VSSMs

Recent studies [53] argue that visual models do not require a causal mode (*i.e.*, the SSM mechanism) for effective task understanding, as most classification datasets (*e.g.*, small-scale images) lack long-sequence dependencies. In response, they propose GatedCNN, a model composed of stacked Gated CNN blocks (see Figure 9), which consistently outperforms VSSMs across various image sizes in classification tasks. Building on prior architectures such as ConvNeXt [31] and InceptionNeXt [54], GatedCNN achieves both simplicity and strong performance. The key distinction between VSSMs and GatedCNN lies in their design: while VSSMs depend on sequence memorization, stacked CNN blocks in GatedCNN offer greater versatility and efficiency in feature extraction.

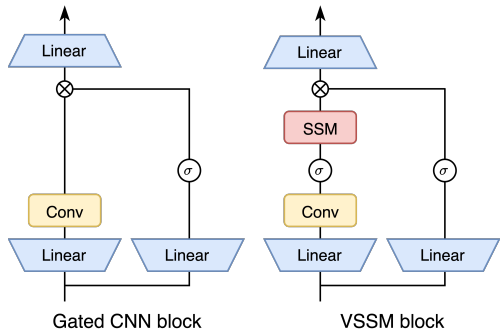


**Figure 9:** Difference between Gated CNNs and VSSM block. For simplicity, we omit the normalization and the shortcut.

Based on our preceding discussion, we summarize our observations regarding the necessity of SSM robustness against backdoor attacks as follows:

- ACC robustness on benign data: VSSM < Gated CNNs
- ASR sensitivity: VSSM >> Gated CNNs
- Gap between ACC and ASR: VSSM < Gated CNNs